PNAS RESEARCH ARTICLE | ENVIRONMENTAL SCIENCES
EARTH, ATMOSPHERIC, AND PLANETARY SCIENCES

Hydrogen isotope fractionation is controlled by CO_2 in coccolithophore lipids

Ismael Torres-Romero[a,1,2], Hongrui Zhang[a,1,2], Reto S. Wijker[a], Alexander J. Clark[a], Rachel E. McLeod[a], Madalina Jaggi[a], and Heather M. Stoll[a]

Edited by Mark Thiemens, University of California San Diego, La Jolla, CA; received October 26, 2023; accepted May 21, 2024

Hydrogen isotope ratios (δ^2H) represent an important natural tracer of metabolic processes, but quantitative models of processes controlling H-fractionation in aquatic photosynthetic organisms are lacking. Here, we elucidate the underlying physiological controls of $^2H/^1H$ fractionation in algal lipids by systematically manipulating temperature, light, and CO_2(aq) in continuous cultures of the haptophyte *Gephyrocapsa oceanica*. We analyze the hydrogen isotope fractionation in alkenones ($\alpha_{alkenone}$), a class of acyl lipids specific to this species and other haptophyte algae. We find a strong decrease in the $\alpha_{alkenone}$ with increasing CO_2(aq) and confirm $\alpha_{alkenone}$ correlates with temperature and light. Based on the known biosynthesis pathways, we develop a cellular model of the δ^2H of algal acyl lipids to evaluate processes contributing to these controls on fractionation. Simulations show that longer residence times of NADPH in the chloroplast favor a greater exchange of NADPH with ^2H-richer intracellular water, increasing $\alpha_{alkenone}$. Higher chloroplast CO_2(aq) and temperature shorten NADPH residence time by enhancing the carbon fixation and lipid synthesis rates. The inverse correlation of $\alpha_{alkenone}$ to CO_2(aq) in our cultures suggests that carbon concentrating mechanisms (CCM) do not achieve a constant saturation of CO_2 at the Rubisco site, but rather that chloroplast CO_2 varies with external CO_2(aq). The pervasive inverse correlation of $\alpha_{alkenone}$ with CO_2(aq) in the modern and preindustrial ocean also suggests that natural populations may not attain a constant saturation of Rubisco with the CCM. Rather than reconstructing growth water, $\alpha_{alkenone}$ may be a powerful tool to elucidate the carbon limitation of photosynthesis.

alkenone | hydrogen isotope fractionation | coccolithophore | CO_2 | carbon concentrating mechanism

Significance

The $^2H/^1H$ ratio of marine algal lipids has been proposed to serve as a chemical fossil of the $^2H/^1H$ ratio of the ocean, tracking changes in the environmental water cycle and ocean salinity. Yet, our culture experiments and a numerical model of cellular H sources in lipid synthesis reveal how the CO_2 concentration and temperature strongly affect the hydrogen isotopic fractionation of acyl lipids by altering the photosynthetic fixation rate and nicotinamide adenine dinucleotide phosphate hydrogen (NADPH) residence time in the chloroplast. This suggests that hydrogen isotope fractionation in acyl lipids may provide insight into the modern and past cellular regulation of algal photosynthesis and the carbon concentrating mechanism.

The stable isotope composition of hydrogen of lipids produced by photosynthetic organisms has often been employed to estimate variations in the isotopic composition of the growth water to reconstruct the hydrological cycle over time (1, 2) because lipid C-H bonds do not further exchange with environmental water after biosynthesis. Lipids feature a lower $^2H/^1H$ than the growth water, and a complication is that the magnitude of this $^2H/^1H$ fractionation depends strongly on physiological factors that change from one compound to another, among species and among different environmental conditions within a given species (3, 4).

Experimental studies have evaluated the influence of several growth conditions on algal lipid hydrogen isotope fractionations relative to growth water. Fractionation is typically expressed by the fractionation factor α, where a lower α indicates more deuterium (^2H or D)-depleted lipids relative to the hydrogen isotope ratio of growth water. In freshwater green algae harvested in the range from 15 to 25 °C, increasing temperature intensifies $^2H/^1H$ fractionation in acyl lipids, lowering α (5). Higher salinity led to higher α in the acyl lipids of the haptophyte *Emiliania huxleyi* (6), and increasing light intensity in cultures led to higher α-values in the acyl lipids of marine diatom *Thalassiosira pseudonana* and in *E. huxleyi* (7, 8). In chemostat cultures, as cell growth rates were slowed by progressive N- or P-nutrient limitation, hydrogen isotope fractionation of acyl lipids in *E. huxleyi* decreased (9). However, apparent discrepancies between the influence of a given environmental factor in culture and natural samples, such as contrasting temperature influence (10) or much higher (11) sensitivity to salinity, challenge simple empirical explanations of the controls on fractionation.

The overall deuterium depletion of algal biomass relative to the water (12) has its root in the large kinetic isotope effect (KIE) of NADPH generation via the ferredoxin-$NADP^+$ reductase (FNR) enzyme at the photosystem I (PSI) of the chloroplast, with an apparent fractionation ($\delta^2H_{NADPH/PSI}$) of around −600‰ from growth water (13). NADPH produced through other pathways, such as the oxidative pentose phosphate pathway (oxPPP),

Author affiliations: [a]Climate Geology, Department of Earth Sciences, ETH Zürich, Zurich 8092, Switzerland

Author contributions: I.T.-R., H.Z., and H.M.S. designed research; I.T.-R., H.Z., R.S.W., A.J.C., R.E.M., M.J., and H.M.S. performed research; H.Z. and R.S.W. contributed new reagents/analytic tools; I.T.-R., H.Z., and H.M.S. analyzed data; and I.T.-R., H.Z., and H.M.S. wrote the paper.

The authors declare no competing interest.

This article is a PNAS Direct Submission.

[1]I.T.-R. and H.Z. contributed equally to this work.

[2]To whom correspondence may be addressed. Email: ismael.torres@erdw.ethz.ch or zhh@ethz.ch.

This article contains supporting information online at https://www.pnas.org/lookup/suppl/doi:10.1073/pnas.2318570121/-/DCSupplemental.

Published June 21, 2024.

is less depleted, with a $\delta^2H_{NADPH/oxPPP}$ around −250‰ (9), consistent with the observation that heterotrophy leads to ^2H-enriched biomass compared to phototrophic growth in plants (14, 15). Consequently, previous explanations (9) proposed that algal lipid $^2H/^1H$ fractionation depends on the relative flows of photosynthetic ^2H-depleted NADPH, extrachloroplastic NADPH, and exchange with intracellular ^2H-enriched water. Another potential mechanism attenuating this strongly negative chloroplastic δ^2H_{NADPH} could be NADPH exchange with intracellular water. This process has been observed during ^2H-labeling experiments in eukaryotic cell lines catalyzed by flavin-dependent enzymes such as glutathione reductase (16) and could change δ^2H_{NADPH} in the chloroplast directly. Yet, despite wide interest in δ^2H application in algal systems, a quantitative evaluation of these hypotheses has not been performed.

Here, to elucidate the underlying physiological controls of fractionation, we provide a set of experimental data from algal lipids grown in continuous culture, in which we systematically manipulate temperature, light, and CO_2(aq). We focus on a specific lipid class, the alkenones, which are ketone alkenes commonly C_{37}/C_{40}-long and di- or triunsaturated. These biomarkers are unique to certain haptophyte algae, allowing their $^2H/^1H$ signal to be attributed to a specific group among mixed populations in the ocean. Alkenones are hypothesized to form from fatty acid precursors synthesized in the chloroplast that would further elongate in the endoplasmic reticulum (17, 18) (*SI Appendix*, Fig. S1). Both alkenones and fatty acids, during their acetogenic synthesis by the multienzyme fatty acid synthase (FAS) complex, obtain almost half of their hydrogen atoms from the redox cofactor NADPH, about a quarter from the precursor acetyl-CoA and the remaining from intracellular water (19, 20). The knowledge of alkenone synthesis allows us to model the variations of $^2H/^1H$ fractionation. Most importantly, alkenones are well-preserved molecular fossils and can be successfully recovered not only from cultures but also from ocean suspended particulate organic matter (SPOM), and marine sediments dating back tens of millions of years (21).

We carried out continuous cultures of *Gephyrocapsa oceanica* RCC1303, an alkenone-producing species contributing significantly to modern and ancient coccolithophore calcite production. Compared with the batch cultures in most previous works, in which increasing cell concentrations progressively deplete dissolved CO_2 levels and increasingly self-shade, steady-state cultures maintain constant cell density. Continuous cultures therefore maintain a more stable CO_2 and light environment, which facilitates full separation of the different environmental influences on $\alpha_{alkenone}$. We also reevaluate whether the influence of CO_2(aq), temperature, and salinity on $\alpha_{alkenone}$ in natural environmental samples is coherent with our findings in cultures. To diagnose the processes responsible for the influence of CO_2(aq), temperature, and light on α, we develop a model to simulate the hydrogen isotope ratio of lipids, incorporating the sensitivity of key cellular metabolic rates to temperature, CO_2(aq), and light. Our findings provide a template for the interpretation of alkenone hydrogen isotope ratios as an indicator of physiological response to environmental pressures and thus inform about central metabolic pathways such as photosynthesis.

Hydrogen Isotope Fractionation as a Function of CO_2, Light, and Temperature

Continuous cultures of *G. oceanica* RCC1303 were grown in photobioreactors under a wide range of CO_2(aq) (5 to 90 µM), light intensities (50 to 200 µE), and temperatures (15 to 27 °C) (*SI Appendix*, Figs. S2 and S3 and Table S1). Harvested cells from photobioreactors had alkenone δ^2H values ranging from −241.4 to −313.3‰, reported as abundance-weighted average of methyl ketones C37:3 and C37:2, and ethyl ketone C38:2Et (*SI Appendix*, Fig. S4). The seawater media spanned −72.7 to −76.1‰, resulting in an $\alpha_{alkenone}$ range of 0.743 to 0.821 for our 29 samples (Dataset S1), where the fractionation factor α is defined relative to growth water as detailed in *Material and Methods*.

The impacts of CO_2(aq), light, and temperature on $\alpha_{alkenone}$ are evaluated individually in data subsets in which variation in the other factors is limited (Fig. 1). At 18 °C and a low light of 50 µE, the CO_2(aq) sensitivity of $\alpha_{alkenone}$ is -9.0×10^{-4} µM^{-1}. Remarkably, at higher light intensities of 100 µE and 200 µE, this CO_2(aq) sensitivity is halved: -4.5×10^{-4} µM^{-1} and -5.1×10^{-4} µM^{-1}, respectively (Fig. 1*A*). While we express the sensitivity in linear terms, we cannot exclude the possibility of a logarithmic or other nonlinear dependence of $\alpha_{alkenone}$ on CO_2(aq) from our data. These possibilities will be subsequently explored in our model simulations. Increasing temperature decreases $\alpha_{alkenone}$, with a slope of -4.9×10^{-3} °C^{-1} in experiments at 200 µE light and 8 to 18 µM CO_2(aq) (Fig. 1*B*). In contrast, higher light generally increases $\alpha_{alkenone}$, with the greatest sensitivity of 2.4×10^{-4} µE^{-1} at very high

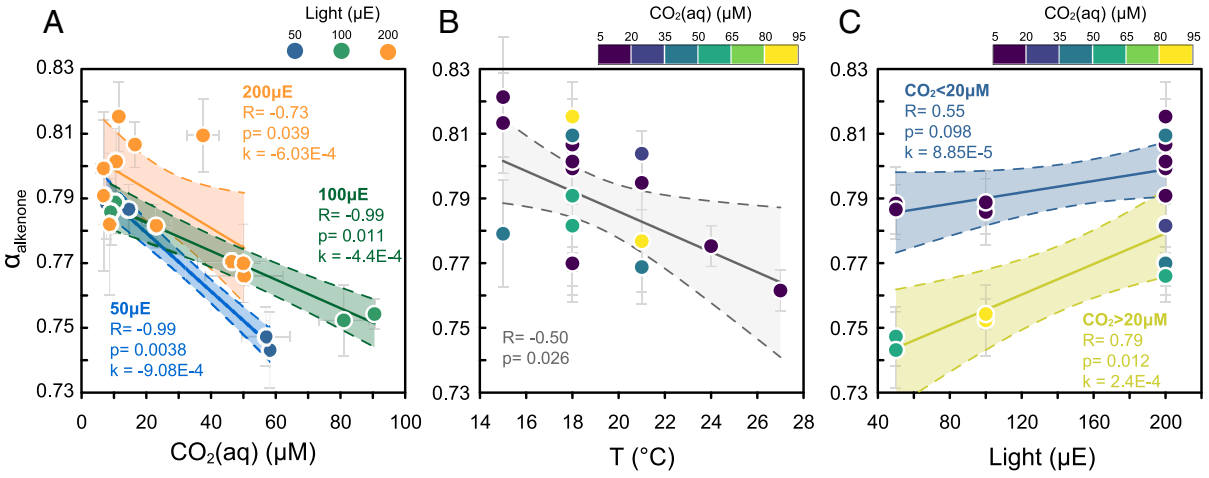

Fig. 1. Alkenone α changes in cultures due to CO_2, temperature, and light. (*A*) CO_2 effect: subset growing at 18 °C in different lights. (*B*) Temperature effect in the subset at 200 µE at different CO_2(aq) levels ($N = 20$). (*C*) Light effect in the subset at 18 °C at different CO_2(aq) ranges. Means of N ≥ 2 and error bars represent one SD. The solid line represents simple regression and dashed lines, 95% CI. The slope of the linear regression is annotated as k and p is the confidence value. It should be noted that the linear relationship between $\alpha_{alkenone}$ and light is insignificant when CO_2 concentration is smaller than 20 µM.

CO_2(aq) levels above 20 µM, and no sensitivity to light at low 5 to 20 µM CO_2(aq) (Fig. 1*C*).

Multiple linear regressions (MLR) were also carried out to account for the combination of the above environmental influences on $\alpha_{alkenone}$ (*SI Appendix*, Table S2). The best prediction of $\alpha_{alkenone}$ using environmental parameters had an R^2 of 0.615:

$$\alpha_{alkenone} = 0.8526 - 6.017\,10^{-4} C_e + 8.815 \cdot 10^{-5} \mathrm{L} - 3.566 \cdot 10^{-3} \mathrm{T}. \quad [1]$$

Using a log(CO_2) in MLR results in a comparably strong prediction of $\alpha_{alkenone}$ (R^2 = 0.58):

$$\alpha_{alkenone} = 0.8807 - 3.672 \cdot 10^{-4} \log(C_e) + 1.258 \cdot 10^{-4} \mathrm{L} - 3.714 \cdot 10^{-3} \mathrm{T}, \quad [2]$$

where CO_2(aq) (C_e), light (L), and temperature (T) have units of µM, µE, and °C, respectively. These regressions highlight the complex relationship between environment parameters and hydrogen isotope ratios in lipids.

In addition to media carbonate system and lipid hydrogen isotope ratios, a large array of biological parameters were analyzed to characterize algal composition (*SI Appendix* and Dataset S1). We performed a cross-correlation analysis (*SI Appendix*, Fig. S5) to gain insight into the different relationships among all the cellular and environmental variables. Along with the previously described correlation of $\alpha_{alkenone}$ to CO_2(aq) (Pearson r = –0.623, *P*-value < 0.001) and light intensity as previously reported (7), we also find that lower $\alpha_{alkenone}$ correlates with higher alkenone content (Pearson r = –0.650, *P*-value = 0.002) and higher calcification (Pearson r = –0.571, *P*-value = 0.003). To a lesser extent, chlorophyll per cell also correlates to lower $\alpha_{alkenone}$. These correlations indicate that the extracellular environmental variations could influence $\alpha_{alkenone}$ via metabolic processes such as photosynthesis and carbon fixation. We do not find any significant correlation between growth rate and $\alpha_{alkenone}$ in our culture data (*SI Appendix*, Fig. S6).

Temperature and CO_2 Influence on $\alpha_{alkenones}$ in Previous Culture and Environmental Samples

Previous culture studies of $\alpha_{alkenone}$ have not focused on manipulating CO_2(aq) and only one prior culture experiment of *E. huxleyi* cultures (22) reported carbon system parameters, namely pH and alkalinity at the start and end of the batch culture. For this experiment, we estimate CO_2(aq) and find a weak negative correlation between $\alpha_{alkenone}$ and average CO_2(aq) [Fig. 2*A* in green, *SI Appendix*, Fig. S7*A*; basis of CO_2(aq) calculation in *SI Appendix*, Table S2]. In cultures with no reported carbon system measurements, it is possible that manipulations of culture temperature, salinity, and culture alkalinity, as well as differences in cell growth rate and cell density at harvest, have also led to systematic variation of CO_2(aq) which has contributed to some reported variations in $\alpha_{alkenone}$ (*SI Appendix, SI Materials and Methods*).

Where environmental samples with published $\alpha_{alkenone}$ originated in regions of the ocean characterized by air–sea CO_2 equilibrium, we estimated the CO_2(aq) characterizing surface ocean environments above published core-top sediments (24) and surface particulate organic matter, SPOM, samples from the euphotic zone (23) (*SI Appendix*, Table S3). In these sets of samples, $\alpha_{alkenone}$ negatively correlates with CO_2(aq) (Fig. 2 and *SI Appendix*, Fig. S7). In both of these sample sets, the range in CO_2(aq) results only from the higher solubility of CO_2 in colder ocean surface waters, and therefore $\alpha_{alkenone}$ is also significantly positively correlated with SST (*P* = 0.0001 for SPOM, *P* = 0.0009 for core-tops), as described previously (22). However, in our cultures, where the CO_2(aq) and temperature vary independently, $\alpha_{alkenone}$ correlates negatively with temperature, as found in several other culture studies (25–27) (Fig. 2*B* and *SI Appendix*, Fig. S7*E*). Therefore, the spatial gradients in α in the ocean are consistent with the sign of α covariation with CO_2(aq) in cultures but inconsistent with sign of α covariation with temperature in cultures. While our cultures exhibit a decrease of $\alpha_{alkenone}$ with rising CO_2 for a single *G. oceanica* strain, the prevalence of similar inverse relationships in natural ocean populations suggests that the main physiological drivers of the relationship are not unique to this *G. oceanica* strain.

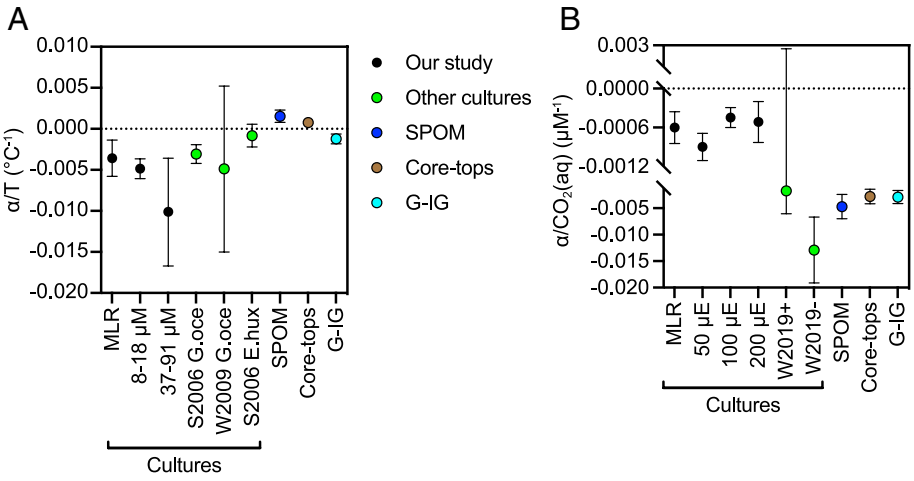

Fig. 2. Comparison between $\alpha_{alkenone}$ in this work and in published datasets. (*A*) Comparison of linear regressions of $\alpha_{alkenone}$ on CO_2(aq) (µM). Slopes cover a CO_2(aq) range of 5 to 90 µM for our MLR. Culture 50, 100, and 200 µE are the slopes calculated on our data subset at 18 °C and indicate light intensity. W2019 is the slope for Weiss et al. cultures (22) at a range from 5.4 to 10.3 µM (excluding Exp. 6, W2019-) or to 12.8 µM (including Exp. 6 datapoint, W2019+). SPOM, surface ocean suspended particulate organic material, is the slope at the 10 to 16 µM range for Gould et al. (23). Core-tops are surface sediments (0 to 1 cm) between 7 and 14 µM from Weiss et al. (24). G-IG, glacial-interglacial, are deep ocean sediments from present-153.1 ky from the Chile margin, and have a range of 7 to 11 µM (11). (*B*) Comparison of linear regressions of $\alpha_{alkenone}$ on temperature (°C). Slopes cover a temperature range of 15 to 27 °C for the MLR of our culture study. Cultures in the CO_2(aq) range of 8 to 18 or 37 to 91 µM are all at 200 µE. S2006 *G. oce* are *G. oceanica* cultures from Schouten et al. (25), W2009 *G. oce* are also *G. oceanica* cultures from Wolhowe et al. (26) and S2006 *E. hux* are *E. huxleyi* cultures from Schouten et al. (25). Datapoints represent slopes and error bars are 95% CIs (*Materials and Methods*).

Over late Pleistocene glacial cycles, glacial periods of low atmospheric CO_2 coincide with low temperature, as well as high ice volume and salinity. Based on our cultures and previous results on salinity (6, 10), all of these factors could contribute to higher $\alpha_{alkenone}$ during glacial times. Previous studies find larger magnitude increases in δ^2H alkenone during glacial time periods (11, 28) than would be expected given modest ocean salinity changes. Low temperature and low CO_2(aq) might be additional drivers of high glacial $\alpha_{alkenone}$; $\alpha_{alkenone}$ vs. CO_2(aq) is negative in slope similar to that of the cultures, assuming sites were at air–sea equilibrium and using CO_2 solubility from alkenone SST and SSS from ice volume (Fig. 2).

Mechanism of $\alpha_{alkenone}$ Varying with CO_2, Temperature, and Light

Our results highlight an influence of CO_2(aq) on δ^2H fractionation, in addition to temperature and light influences on fractionation. Previous conceptual explanations for variable fractionation proposed that algal lipid $^2H/^1H$ fractionation depends on the relative flows of photosynthetic ^2H-depleted NADPH, extrachloroplastic NADPH, and exchange with intracellular ^2H-richer water (9), i.e., the major source of alkenone and fatty acid δ^2H is the hydrogen transferred during the redox reactions to $NADP^+$. We extend this conceptual mechanism by considering the enzymatic H exchange between the ^2H-depleted NADPH in the chloroplast with H_2O by flavoproteins (16) (Fig. 3*A* and *SI Appendix*, Fig. S1). We hypothesize that the activity level of these enzymes and the turnover of the generated NADPH determine its residence time in the chloroplast (τ_{NADPH}). The NADPH residence time, τ_{NADPH}, is defined as the NADPH amount in chloroplast divided by the NADPH generation rate or consumption rate with a unit of second (*SI Appendix*, Eq. **S38**). A longer NADPH residence time would allow a more exchange with the heavier isotopic intracellular water, leading to more positive $\delta^2H_{NADPH,x}$, and thereby larger $\alpha_{alkenone}$ (15). We therefore propose that the $\tau_{NADPH,x}$ is the major factor controlling hydrogen isotope fractionation of alkenones, and the residence time is systematically affected by the CO_2(aq), temperature, and light conditions which regulate the photosynthetic process.

To test our hypothesis, we construct a numerical model (*SI Appendix*, *SI Material and Methods*) to simulate how environmental factors affect the variations of cell metabolism causing hydrogen isotope fractionations in lipids. The model focuses on the key processes influencing hydrogen isotope ratios of NADPH in chloroplast (Fig. 3*A* and *SI Appendix*, Fig. S8) and reproduces several important aspects of the observations in experiments (Fig. 3*B*). First, at constant temperature, the negative correlation between CO_2(aq) and $\alpha_{alkenone}$ is well reproduced in simulations. Second, a larger $\alpha_{alkenone}$ characterizes high light conditions in both simulation and laboratory culture. Third, the model captures the higher sensitivity of $\alpha_{alkenone}$ to light under high CO_2 conditions, while the light effect is negligible in a low CO_2 environment.

We can diagnose that these responses are driven by variations in $\tau_{NADPH,x}$ (Fig. 4). Higher CO_2(aq) and higher temperature can decrease the $\tau_{NADPH,x}$ by enhancing the carbon fixation rate and lipid synthesis rate (red fluxes in Fig. 4*A*). In this case, the consumption rate of NADPH is higher than the NADPH-water exchange rate (Fig. 4*A*). Thus, higher CO_2(aq) and higher temperature result in stronger fractionations (more negative $\delta^2H_{alkenone}$ and lower $\alpha_{alkenone}$). More generally, a higher carbon fixing rate and hydrogen exchange rate ratio (F_3/F_2 in Figs. 3 and 4) leads to lower $\alpha_{alkenone}$, which would also enhance alkenone content. That could explain the inverse correlation between $\alpha_{alkenone}$ and the cellular alkenones/POC (*SI Appendix*, Fig. S5).

Light fuels the photosynthetic chain providing the energy to reduce the $NADP^+$ stromal pool and keeps a high NADPH/NADP ratio in the chloroplast (29). A higher NADPH concentration would increase the residence time of chloroplast NADPH (*SI Appendix*, Eq. **S38**),

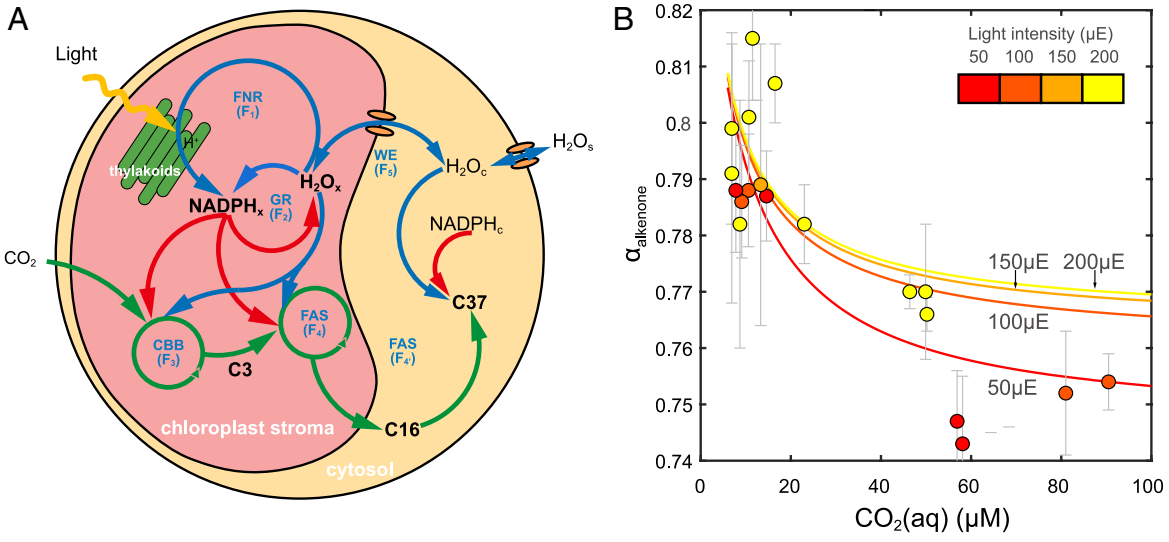

Fig. 3. Model structure and comparison between simulations and laboratory cultures. (*A*) Structure of the hydrogen fractionation model in this work. There are two simulated compartments: the chloroplast and cytoplasm. The hydrogen isotope ratios of NADPH in chloroplast ($NADPH_x$), intracellular water (H_2O_x and H_2O_c), production of small C3 carbon metabolites, fatty acid precursors from chloroplast (C16), and alkenones from cytoplasm (C37) are simulated. In different colors, the six fluxes affecting the hydrogen isotope ratios of alkenones are highlighted: in red, fluxes using NADPH as a substrate; in green, fluxes using carbon molecules, and in blue, fluxes with water. The ferredoxin-NADP reductase (FNR) introduces a δ^2H in $NADPH_x$ of −600‰ relative to the stromal water (H_2O_x) (flux F_1). This ^2H-depleted H from $NADPH_x$ exchanges with the ^2H-enriched H_2O_x via flavoproteins such as glutathione reductase (GR) (fluxes F_2). $NADPH_x$ is mainly consumed by the CBB cycle and the FAS complex (fluxes F_3 and F_4), whose competition with flavoproteins (GR) determines NADPH residence time (τ_{NADPx}). The CBB produces C3 compounds that can generate acetyl-CoA for fatty acid production by the FAS. These fatty acids can be exported to the cytoplasm for further elongation to produce alkenones. The different H_2O channels and pumps influence the water δ^2H by exchanging water (WE) between the chloroplast and cytoplasm (fluxes F_5). (*B*) Comparison between simulation and laboratory culture results on CO_2(aq) and light effect at 18 °C. The lines are simulation results at fixed 18 °C temperature at varying CO_2(aq). The circles are measurements in laboratory culture. Gray bars represent the SD of hydrogen isotope fractionations calculated from C37:3, C37:2, and C38:2Et alkenones ($\alpha_{alkenone}$). Only the cultures carried out at 18 °C are presented in this panel to remove the temperature effect. The color of circles and lines represents the light intensity in μE and shares the same colormap.

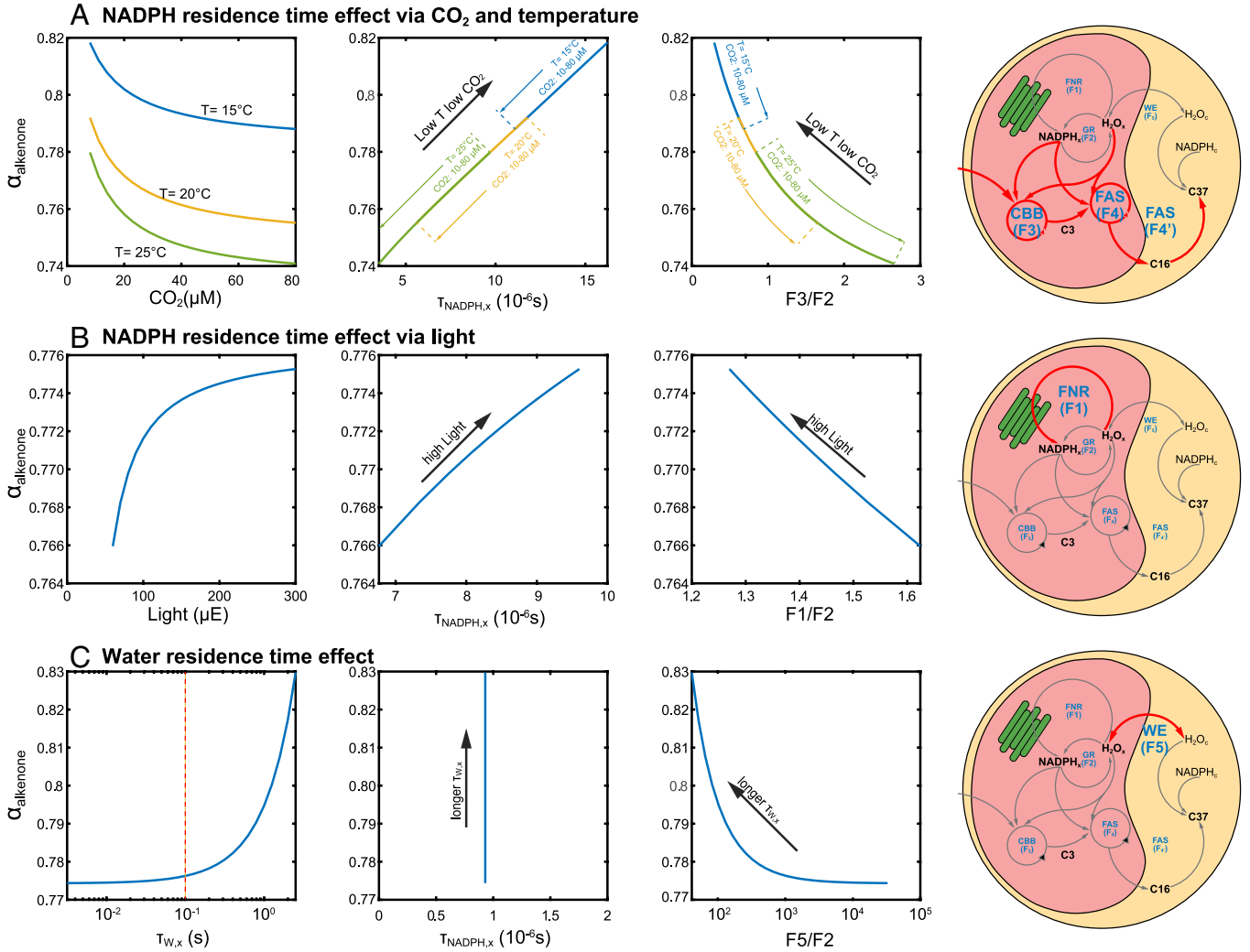

Fig. 4. Sensitivity tests on temperature, CO_2(aq), light, and water residence time on $\alpha_{alkenone}$. (*A*) Simulating faster alkenone synthesis at high CO_2(aq) and/or high temperature. The different lines represent simulated $\alpha_{alkenone}$ as a function of CO_2(aq) at increasing temperatures (1st panel), as a function of NADPH residence time in the chloroplast (2nd plot) and as a function of the ratio between simulated fluxes 3 and flux 2 (3rd plot). It should be noted that the lines of different temperature and CO_2(aq) combinations in the 2nd and 3rd panels are overlapping. This overlap results from dual temperature and CO_2 control on carbon fixation rate which affects hydrogen isotope fractionation. (*B*) Simulating faster $NADPH_x$ reduction at high light intensity. Here, the *Left* panel shows $\alpha_{alkenone}$ in function of the ratio between simulated fluxes 1 and 2 (F1/F2). The red line in the *Right* panel represents the generation of NADPH is enhanced in high light conditions. (*C*) Simulating lower water residence time at slow water exchange between chloroplast and cytoplasm. Here, the 3rd panel shows $\alpha_{alkenone}$ in function of the ratio between simulated fluxes 5 and 2 (F5/F2). The red lines in the right cell diagram represent enhanced carbon fixation and lipid synthesis in high temperature and high CO_2 conditions.

allowing more time for hydrogen exchange between water and NADPH (Fig. 4*B*). Therefore, a higher light intensity results in a smaller fractionation and a higher $\alpha_{alkenone}$. As illustrated in Fig. 1*C*, the light effect is muted at very low CO_2(aq) conditions when the consumption of NADPH in the chloroplast is very low due to the CO_2 limitation of the Calvin–Benson–Bassham cycle (CBB). Thus, the NADPH levels in the chloroplast are still very high even during low light conditions (*SI Appendix*, Fig. S9). In this case, the light effect on $\tau_{NADPH,x}$ and $\alpha_{alkenone}$ is not significant. This explanation fits with previous studies with low CO_2/high light conditions suggesting that light intensity does not have a direct effect on NADPH hydrogen isotopic fractionation (30).

An increase in the abundance of glutathione reductase with higher light could also lead to the light dependence of $\alpha_{alkenone}$. The primary function of glutathione reductase is to maintain the cellular redox balance by catalyzing the reduction of oxidized glutathione to its reduced form using NADPH as a cofactor. This process helps to protect cells from oxidative stress by scavenging reactive oxygen species (31) and maintaining the antioxidant capacity of the cell. Higher content of glutathione reductase can accelerate the exchange of hydrogen between NADPH and water resulting in a smaller fractionation between alkenone and water. Because a high content of glutathione reductase has the same effect as the high NADPH generation rate in high light, these two effects are combined in our model parameterization to reduce the degrees of freedom.

Potential Influences from Other Processes

Salinity correlates positively with $\alpha_{alkenone}$ in some laboratory culture experiments (6, 25), but the detailed mechanism of the salinity effect is still under debate (2). Moreover, most experimental manipulation of culture media salinity has also affected alkalinity, which alters the carbon system and complicates the distinction between the salinity effect and potential CO_2 effects (30). Salinity could play a minor role in lipid hydrogen isotope ratios via changing the water residence time in the chloroplast (τ_W) (32, 33). During $NADP^+$ reduction via FNR, more ^1H goes into NADPH resulting in a more ^2H-enriched chloroplast water. If the chloroplast water has a low exchange rate with external water, thus a longer water residence time in chloroplast ($\tau_{W,x}$), then the enrichment of ^2H would be greater and finally lead to a smaller hydrogen isotope fractionation in alkenones (higher $\alpha_{alkenone}$). Since there is no accurate estimation of the water residence time in

coccolithophores, we test a large range of $\tau_{W,x}$ from 0.01 to 1 s, but we do not suggest that the $\tau_{W,x}$ would vary dynamically in a single cell over such a large range. Based on our simulation, selection of a $\tau_{W,x}$ of 0.001 to 10 s results in $\alpha_{alkenone}$ changing from 0.775 to 0.8, which is equivalent to ~25‰ increase in hydrogen isotope ratio (Fig. 3*C*). The observed change in fractionation correlated with salinity in culture is equivalent to ~5‰ from 25 to 35 practical salinity units (6, 25). This suggests that, if the fractionation change is due to a salinity effect on $\tau_{W,x}$, the variation of $\tau_{W,x}$ with salinity should be in a much narrower range than our sensitivity test. Recent works using surface sediment samples have found that there is only a weak correlation between surface water salinity and $\alpha_{alkenone}$. Thus, the salinity effect on $\alpha_{alkenone}$ could be overwhelmed by other environmental factors, such as light and CO_2, in most of natural samples.

In some chemostat culture experiments under 24-h illumination, as nutrient limitation is relieved and growth rates increase, $\alpha_{alkenone}$ decreases (9). If in these experiments the growth rate is proportional to the gross C fixation rates, this response is consistent with our modeled decrease in $\alpha_{alkenone}$ with higher gross C fixation (Fig. 4*A*) which lowers $\tau_{NADPH,x}$. At the same time, in our experiments (*SI Appendix*, Fig. S6) and across all published datasets reporting growth rate, there is no significant correlation between growth rate and $\alpha_{alkenone}$ (*SI Appendix*, Fig. S10). One explanation is that the balance of gross photosynthetic fixation and respiration may vary under different experimental conditions, decoupling measured cell growth rates from gross C fixation and decoupling $\alpha_{alkenone}$ from growth rate.

Our model accounts for the core processes in chloroplast affecting $\alpha_{alkenone}$, which are more related to the carbon fixation, and simulates the main trends in the dataset (*SI Appendix*, Fig. S11). Other sources of $NADP^+$ reduction from respiration, such as the tricarboxylic acid cycle and the oxidative pentose phosphate pathway (oxPPP), are not simulated in our model. The NADPH generated in chloroplast and cytoplasm could also exchange with each other via malic acid shuttle and triose phosphate shuttle to meet metabolic needs (34). Thus, the source of NADPH can also vary with cellular metabolic processes. For example, nutrient limitation might decrease growth rate and increase respiration rate, resulting in a higher oxPPP contribution and increasing the hydrogen isotope ratios of lipids as suggested by Sachs and Kawka (9).

Further complexity could be added to the model to evaluate the effects of oxPPP contributing to the isotope composition of NADPH (35), for example, by allowing fractionation between NADPH and water in chloroplast ($\alpha_{w\text{-}N,x}$) to vary with the fraction of oxPPP involvement. If the oxPPP contribution were constant, it would affect the absolute value of $\alpha_{alkenone}$, and would affect our parameter tuning, but it would not affect the $\alpha_{alkenone}$ response to environmental variables. On the other hand, if the relative contribution of the oxPPP were variable, it could contribute to variation in $\alpha_{alkenone}$ in response to environmental variables like CO_2. Implementation into the model would require independent constraints on the drivers of the varying relative contribution of the oxPPP.

It should be noted that some KIE used in our simulations (*SI Appendix*, Table S5) are also not well constrained by independent experimental data, which could increase the uncertainty of our simulations. Also, the model is limited to acyl lipids, and quantitative simulation of α in other biosynthesis pathways may require additional model complexity.

Implications of $\alpha_{alkenone}$-CO_2 Sensitivity on CCMs

In our reference simulations illustrated in Figs. 3 and 4, we set the CO_2(aq) at the site of Rubisco ($CO_{2,x}$) as 1.5 fold higher than the CO_2(aq) in the seawater. An assumption of elevated CO_2 at the site

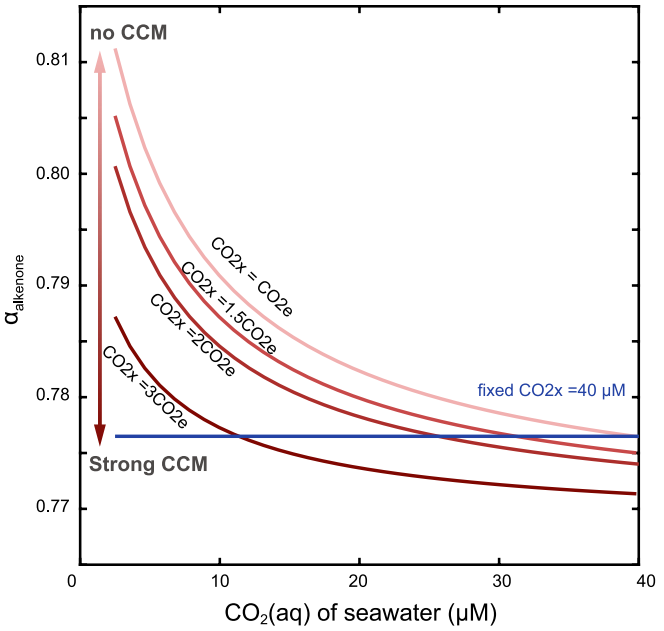

Fig. 5. Influence of CCM strategies on $\alpha_{alkenone}$. The intensity of CCM affects CO_2 concentration in the chloroplast (CO2x). The pink lines represent different intensities of CCM resulting in a varying CO2x and thereby different $\alpha_{alkenone}$. The left arrow shows the CCM intensity from non-CCM to strong CCM. The blue line represents that $\alpha_{alkenone}$ does not respond to CO_2(aq) if the cells employ a constant CCM (set as 40 μM in this test).

of photosynthesis compared to that in extracellular media is consistent with evidence that coccolithophores, like many other eukaryotic and prokaryotic algae, can operate a CO_2-concentrating mechanism (CCM) (36–38). However, there is as of yet no direct means to quantify the degree of CO_2 enhancement at the site of Rubisco by a growing cell. A limited number of studies on diatoms provide indirect estimations of the CO_2 at the site of photosynthesis from modeling gas fluxes during incubations but are subject to significant uncertainties (39–41).

An optimal CCM would be expected to maintain the $CO_{2,x}$ at a level nearly saturating Rubisco, such that at a given temperature, the $CO_{2,x}$ would be constant regardless of external CO_2(aq). We have simulated such a case of a CCM at constant saturation and find that, in this case, $\alpha_{alkenone}$ would be insensitive to CO_2(aq) during culture (blue lines in Fig. 5). Thus, the persistent decline in $\alpha_{alkenone}$ with an increase of external CO_2(aq) in, not only our culture experiments (Fig. 1*A*), but also the global surface sediment samples (Fig. 2), indicates that these alkenone producers do not feature a CCM fully up-regulating to attain a constant saturation of Rubisco. At the same time, at constant temperature and light, a portion of the variability in $\alpha_{alkenone}$ for a given CO_2(aq) may be caused by different intensity of the CCM and the CO_2(aq) of the chloroplast (Fig. 5).

Our finding of an unsaturated CCM is consistent with previous field measurements which indicate that the high energetic cost of CCM operation may lead to running the CCM at a lower intensity (40). Previous field experiments suggested that the CCM may not operate close to saturation in cold conditions due to the low enzyme turnover rates (41). However, our results at 18 °C suggest that the limited operation of a CCM may be a more general strategy, not only at cold temperature. Indeed, the persistent inverse correlation of $\alpha_{alkenone}$ with CO_2(aq) in the modern and preindustrial ocean (Fig. 2*A*) also suggests that natural populations may not attain a constant saturation of Rubisco through the CCM. Furthermore, the apparent sensitivity of $\alpha_{alkenone}$ to CO_2(aq) variations for the past 153 ky (*SI Appendix*, Fig. S7) may indicate that the CCM has not been fully up-regulated to compensate for glacial minima in CO_2(aq), an

observation important to document in additional locations of expected air–sea equilibrium.

Our results also provide additional constraints on the role of light in the CCM. Previous studies suggested that higher light intensity may lead to higher $CO_{2,x}$ by providing energy for the CCM or via light-dependent transporters (42, 43). If this mechanism were dominant, then higher light would lead to lower $\alpha_{alkenone}$ by enriching $CO_{2,x}$ concentrations (red lines in Fig. 5) and increasing the carbon fixation rate (Fig. 3*A*). In contrast, our data suggest that higher light may not be ubiquitously correlated to higher $CO_{2,x}$, or that a $CO_{2,x}$ enrichment could be masked by high NADPH concentrations. Future studies with experimental CO_2 conditions spanning the CO_2(aq) range of highest model sensitivity of $\alpha_{alkenone}$ and including additional strains of alkenone producers could be used to more clearly elucidate the CCM via hydrogen isotopic fractionations of lipids.

Conclusions

Our culture results document an important influence of CO_2 on $\alpha_{alkenone}$ which suggests that $\alpha_{alkenone}$ may not be suited for simple application as a proxy for salinity. The positive covariation of salinity and temperature, and their inverse correlation with CO_2 spatially in the modern ocean complicates efforts to empirically derive the dependence of $\alpha_{alkenone}$ on any one of these variables purely from core-top or SPOM measurements. Future culture studies carefully controlling for carbon system variation may improve constraints on the direct temperature and salinity effects in a broader range of alkenone-producing species and strains. If the temperature effect is similar and reproducible across species, it may be possible to account for its influence on α in studies on environmental samples. At the same time, our simulations indicate that the NADPH residence time in the chloroplast is a dominant control on $\alpha_{alkenone}$. Thus, rather than a passive recorder of environmental parameters, $\alpha_{alkenone}$ may be well suited to provide a key perspective on the cellular regulation of photosynthesis and the CO_2 availability in the chloroplast in the modern and past oceans.

Materials and Methods

Continuous Cultivation. *Gephyrocapsa oceanica* RCC1303 (Roscoff Culture Collection) cells were inoculated into 1 or 3-L photobioreactors (FMT150, Photon Systems Instruments) aerated at different pCO_2 levels. Light intensity of a cool-white LED panel was set in sinusoid mode for a diurnal rhythm of 8 h dark/16 h light plateauing at 50 to 200 μE (*SI Appendix*, Fig. S3). An array of different combinations of temperature, pCO_2, and light (*SI Appendix*, Fig. S2 and Table S1) was imposed to grow 29 cultures. Photobioreactors were operated in turbidostat mode by automatic dilution triggered above an optical density at 680 nm (OD680) equivalent to 1 to 2×10^5 cells mL^{-1} (log phase). Cells were kept in suspension with gentle magnet stirring, air BUBBLING, and thorough daily manual resuspension of precipitate cells. More details about cell density, carbonate system control, and particulate organic/inorganic carbon measurements, lipids extraction, and identifications can be found in *SI Appendix*.

Hydrogen Isotope Analysis. The stable hydrogen isotopic compositions of alkenones were analyzed by a gas chromatograph (Thermo Scientific Trace GC Ultra) coupled to an isotope ratio mass spectrometer (Thermo Scientific Delta V) using a pyrolysis interface (Thermo Scientific Isolink). Samples were injected with a GC PAL autosampler system (CTC Analytics AG) in splitless mode with a PTV injector (Gerstel CIS 6). Helium gas with a flow rate of 1 mL/min was used as the carrier gas. Separation of alkenones was performed with a 105 m × 0.32 mm capillary column (Rtx-200, 0.5 μm film thickness, Restek) with the following temperature program: 1 min at 50°, temperature gradient of 25 °C min^{-1} to 250 °C and 2 °C min^{-1} to 305 °C, hold for 25 min, then to 310 °C at 10 °C min^{-1} and hold for 5 min. For each sample, triplicate measurements were performed to determine the δ^2H value of alkenones and FAMEs, respectively, and reported as per mil relative to Vienna Standard Mean Ocean Water (VSMOW). Our in-house alkenones standard and A7 (purchased from Indiana University) were used as standards.

Water hydrogen isotope ratios were analyzed on a Picarro L2120-*i* cavity ringdown spectrometer using reference waters SLAP2, GRESP, and VSMOW2. Accuracy (2σ) for δ^2H was 1‰ based on reproducibility of 6 measurements of international standard USGS W-67400-S. The apparent lipid-water fractionation factor α was calculated as

$$\alpha_{alkenone} = \frac{\delta^2H_{alkenone} + 1000}{\delta^2H_{water} + 1000}, \quad [3]$$

where δ^2H_{lipid} is the weighted average of the most abundant alkenone species: methyl ketones C37:3 and C37:2 and ethyl ketone C38:2Et. The δ^2H of each alkenone is shown in *SI Appendix*, Fig. S4. The three alkenones show very similar α. Thus, further α analysis applies to the abundance-weighted average of the three alkenones and only for the cultures with a low analytical error (SD <3%). This allowed us to calculate a reproducible δ^2H across all samples, because for cases where one of these three alkenones was too low in abundance for precise isotopic measurement, its low abundance would preclude the alkenone having appreciable influence on the weighted average isotopic value.

Inferring CO_2(aq) from Other Studies. The approach for calculation of CO_2(aq) from environmental samples and from one culture is summarized in *SI Appendix*, Table S2. For cultures from Weiss et al. (22), CO_2(aq) was estimated from CO2SYS excel macro (44) based on reported alkalinity and pH, and using the total scale, 35‰ salinity, 7 μM phosphate, and 0 μM silicate. From these *E. huxleyi* batch cultures (22), we included data where calculated CO_2(aq) variations from initial to final measurement varied by <5 μM. Among these experiments, we compared the 11 cultures with similar cell growth effect on alkalinity (consumed by 238 ± 118 μM) (conditions 1 to 5). For environmental samples, we used the temperature-dependent solubility and equilibrium with atmosphere of 280 ppmv for core-tops and 400 ppm for recent suspended particulate matter. The CO_2 ranges of environmental samples are in the lower range (7 to 16 μM) of our culture samples (5 to 90 μM), and we cannot determine the nonlinearity of the CO_2 effect from our cultures. Consequently, we cannot distinguish whether the CO_2(aq) is higher in environmental samples or whether our culture's linear regression has underestimated sensitivity at the lower range (Fig. 2*A*).

We did not estimate CO_2(aq) from culture experiments in which no carbon system variables were reported. However, CO_2(aq) may have varied in many culture studies, in some cases in systematic ways with the experimentally manipulated variables. Due to the temperature influence on CO_2 solubility, increasing temperature without modifying the carbon chemistry would naturally feature lower CO_2(aq), a situation that will counteract the temperature effect on $\alpha_{alkenone}$ and attenuate its manifestation in cultures, potentially contributing to debate over the importance of temperature in previous culture experiments (22). Because reducing salinity from 35 to 25 g/kg increases CO_2 solubility and CO_2(aq) increases from 14.3 μM to 17.3 μM, $\alpha_{alkenone}$ decreases at lower salinity may also be influenced by the salinity effect on CO_2(aq) solubility. More rigorous quantification of such variation in, for example, alkalinity, may help distinguish salinity from carbon system effects in future studies.

Model Structure. We quantitatively test this hypothesis in a numerical hydrogen isotope model for alkenone producers. Briefly, the model simulates NADPH production during photosynthesis and its subsequent consumption to synthesize alkenones (*SI Appendix*, *SI Materials and Methods*). Production of alkenones (C37) uses the hydrogen from NADPH and water in the cytoplasm by elongating fatty acid precursors (C16) imported from the chloroplast. Both C37 and C16 compounds are made by the FAS complex, but C16 production consumes NADPH and water from the chloroplast and acetyl-CoA. The C16 is derived from the C3 compounds produced during CO_2 fixation by the CBB cycle. We use this framework to test how variations of $\alpha_{alkenone}$ are driven by the dynamics of the chloroplast NADPH hydrogen isotope ratios ($\delta^2H_{NADPH,x}$) and water hydrogen isotope ratios ($\delta^2H_{W,x}$).

The $\delta^2H_{NADPH,x}$ is controlled by the relative intensities of five different metabolic fluxes within the chloroplast (*SI Appendix*, Table S4), which in turn are systematically influenced by temperature, light, and CO_2(aq). Higher light intensity is used to oxidize more water, which increases the linear electron flow of the photosynthetic chain, and passes more electrons on to $NADP^+$, the final electron

acceptor, via the ferredoxin-$NADP^+$ reductase (FNR, F_1 in Fig. 3*A*), increasing the generation rate of NADPH:

$$2 \text{ reduced ferredoxin} + NADP^+ + H^+ \rightarrow 2 \text{ oxidized ferredoxin} + NADPH. \quad [4]$$

This chloroplastic NADPH exchanges with intracellular water via flavoproteins such as glutathione reductase (GR, F_2 in Fig. 3*A*) at a rate dependent on NADPH residence time ($\tau_{NADPH,x}$), which is affected by its redox turnover. The major consumption of NADPH in the chloroplast is the carbon fixation in the CBB cycle (F_3 in Fig. 3*A*), and the fatty acid synthetase (FAS, F_4, and $F_{4'}$ in Fig. 3*A*):

$$3\,CO_2 + 9\,ATP + 6\,NADPH + 5\,H_2O \rightarrow G3P\,(C3) + 9\,ADP + 8\,Pi + 6\,NADP^+ + 2\,H^+, \quad [5]$$

$$8 \text{ acetyl-CoA} + CO_2 + 14\,NADPH + 13\,H^+ + 7\,ATP \rightarrow \text{Palmitate}\,(C16) + 8 \text{ CoA-SH} + 6\,H_2O + 14\,NADP^+ + 7\,ADP + 7\,Pi. \quad [6]$$

The rate of the first reaction (Eq. **5**) is limited by the CO_2(aq) at the site of Rubisco, the core CBB enzyme. In our reference simulation, we estimate that the CO_2(aq) at the site of Rubisco is elevated 1.5-fold relative to the external CO_2(aq) in the seawater, and therefore the consumption of NADPH increases with higher seawater CO_2(aq). We evaluate this CO_2 assumption in a later section. Higher temperature increases the catalytic turnover rate of Rubisco (45), and therefore NADPH consumption. When NADPH turnover is slow, the enzymatic exchange between NADPH and water (F_2) is higher, resulting in a higher $\delta^2H_{NADPH,x}$ value as the initial FNR isotopic depletion in the NADPH is attenuated by exchange with the large H reservoir in chloroplast water. The hydrogen isotopic composition of chloroplast water ($\delta^2H_{W,x}$) is also simulated dynamically (*SI Appendix, SI Materials and Methods*). The hydrogen isotope ratio of water in cytoplasm is assumed to be the same as seawater based on the rapid water exchange facilitated by aquaporins (46). Our model configuration captures the core fluxes and exchanges occurring in the synthesis of acyl lipids such as alkenones and evaluates whether these processes are sufficient to cause the observed variation in $\alpha_{alkenone}$ (*SI Appendix*, Fig. S11).

Data, Materials, and Software Availability. All study data are included in the article and/or supporting information.

ACKNOWLEDGMENTS. We thank Pratigya Polissar for prompting us to assess alkenone δ^2H fractionation as an indicator of light-limited growth. We thank Thomas Blattmann for guiding the Picarro water measurements, and Tim Eglinton and the Biogeoscience group for instrument access and constructive comments on the manuscript. This work was supported by the Swiss NSF (Award 200021_182070 to H.M.S.), ETH Seed Grant (SEED-17 21-2 to I.T.-R.), and ETH core funding.

1. S. N. Ladd *et al.*, Leaf wax hydrogen isotopes as a hydroclimate proxy in the tropical Pacific. *J. Geophys. Res. Biogeosci.* **126**, e2020JG005891 (2021).
2. D. Sachse *et al.*, Molecular paleohydrology: Interpreting the hydrogen-isotopic composition of lipid biomarkers from photosynthesizing organisms. *Ann. Rev. Earth Planet. Sci.* **40**, 221–249 (2012).
3. Y. Huang, B. Shuman, Y. Wang, T. Webb, Hydrogen isotope ratios of individual lipids in lake sediments as novel tracers of climatic and environmental change: A surface sediment test. *J. Paleolimnol.* **31**, 363–375 (2004).
4. Z. Zhang, J. P. Sachs, Hydrogen isotope fractionation in freshwater algae: I. Variations among lipids and species. *Org. Geochem.* **38**, 582–608 (2007).
5. Z. Zhang, J. P. Sachs, A. Marchetti, Hydrogen isotope fractionation in freshwater and marine algae: II. Temperature and nitrogen limited growth rate effects. *Org. Geochem.* **40**, 428–439 (2009).
6. D. M'boule *et al.*, Salinity dependent hydrogen isotope fractionation in alkenones produced by coastal and open ocean haptophyte algae. *Geochim. Cosmochim. Acta* **130**, 126–135 (2014).
7. M. T. J. van der Meer *et al.*, Large effect of irradiance on hydrogen isotope fractionation of alkenones in *Emiliania huxleyi*. *Geochim. Cosmochim. Acta* **160**, 16–24 (2015).
8. J. P. Sachs, A. E. Maloney, J. Gregersen, Effect of light on $^2H/^1H$ fractionation in lipids from continuous cultures of the diatom *Thalassiosira pseudonana*. *Geochim. Cosmochim. Acta* **209**, 204–215 (2017).
9. J. P. Sachs, O. E. Kawka, The influence of growth rate on $^2H/^1H$ fractionation in continuous cultures of the coccolithophorid *Emiliania huxleyi* and the diatom *Thalassiosira pseudonana*. *PLoS One* **10**, e0141643 (2015).
10. B. A. Mitsunaga *et al.*, Alkenone δ2H values–A viable seawater isotope proxy? New core-top δ2HC37:3 and δ2HC37:2 data suggest inter-alkenone and alkenone-water hydrogen isotope fractionation are independent of temperature and salinity. *Geochim. Cosmochim. Acta* **339**, 139–156 (2022).
11. G. M. Weiss *et al.*, Paleosensitivity of hydrogen isotope ratios of long-chain alkenones to salinity changes at the Chile Margin. *Paleoceanogr. Paleoclimatol.* **34**, 978–989 (2019).
12. M. F. Estep, T. C. Hoering, Stable hydrogen isotope fractionations during autotrophic and mixotrophic growth of microalgae. *Plant Physiol.* **67**, 474–477 (1981).
13. Y.-H. Luo, L. Steinberg, S. Suda, S. Kumazawa, A. Mitsui, Extremely low D/H ratios of photoproduced hydrogen by cyanobacteria. *Plant Cell Physiol.* **32**, 897–900 (1991).
14. M.-A. Cormier, R. A. Werner, M. C. Leuenberger, A. Kahmen, ^2H-enrichment of cellulose and *n*-alkanes in heterotrophic plants. *Oecologia* **189**, 365–373 (2019).
15. R. S. Wijker, A. L. Sessions, T. Fuhrer, M. Phan, $^2H/^1H$ variation in microbial lipids is controlled by NADPH metabolism. *Proc. Natl. Acad. Sci. U.S.A.* **116**, 12173–12182 (2019).
16. Z. Zhang, L. Chen, L. Liu, X. Su, J. D. Rabinowitz, Chemical basis for deuterium labeling of fat and NADPH. *J. Am. Chem. Soc.* **139**, 14368–14371 (2017).
17. J.-F. Rontani, F. G. Prahl, J. K. Volkman, Re-examination of the double bond positions in alkenones and derivatives: Biosynthetic implications1. *J. Phycol.* **42**, 800–813 (2006).
18. Y. Zheng, J. T. Dillon, Y. Zhang, Y. Huang, Discovery of alkenones with variable methylene-interrupted double bonds: Implications for the biosynthetic pathway. *J. Phycol.* **52**, 1037–1050 (2016).
19. V. Baillif, R. J. Robins, S. Le Feunteun, P. Lesot, I. Billault, Investigation of fatty acid elongation and desaturation steps in *Fusarium lateritium* by quantitative two-dimensional deuterium NMR spectroscopy in chiral oriented media. *J. Biol. Chem.* **284**, 10783–10792 (2009).
20. J. Baan, M. Holloway-Phillips, D. B. Nelson, A. Kahmen, The metabolic sensitivity of hydrogen isotope fractionation differs between plant compounds. *Phytochemistry* **207**, 113563 (2023).
21. P. Farrimond, G. Eglinton, S. C. Brassell, Alkenones in Cretaceous black shales, Blake-Bahama Basin, western North Atlantic. *Org. Geochem.* **10**, 897–903 (1986).
22. G. M. Weiss *et al.*, Hydrogen isotope fractionation response to salinity and alkalinity in a calcifying strain of *Emiliania huxleyi*. *Org. Geochem.* **134**, 62–65 (2019).
23. J. Gould, M. Kienast, M. Dowd, E. Schefuß, An open-ocean assessment of alkenone δD as a paleo-salinity proxy. *Geochim. Cosmochim. Acta* **246**, 478–497 (2019).
24. G. M. Weiss, S. Schouten, J. S. Sinninghe Damsté, M. T. J. van der Meer, Constraining the application of hydrogen isotopic composition of alkenones as a salinity proxy using marine surface sediments. *Geochim. Cosmochim. Acta* **250**, 34–48 (2019).
25. S. Schouten *et al.*, The effect of temperature, salinity and growth rate on the stable hydrogen isotopic composition of long chain alkenones produced by *Emiliania huxleyi* and *Gephyrocapsa oceanica*. *Biogeosciences* **3**, 113–119 (2006).
26. M. D. Wolhowe, F. G. Prahl, I. Probert, M. Maldonado, Growth phase dependent hydrogen isotopic fractionation in alkenone-producing haptophytes. *Biogeosciences* **6**, 1681–1694 (2009).
27. M. D. Wolhowe, F. G. Prahl, G. Langer, A. M. Oviedo, P. Ziveri, Alkenone δD as an ecological indicator: A culture and field study of physiologically-controlled chemical and hydrogen-isotopic variation in C37 alkenones. *Geochim. Cosmochim. Acta* **162**, 166–182 (2015).
28. S. Kasper *et al.*, Testing the alkenone D/H ratio as a paleo indicator of sea surface salinity in a coastal ocean margin (Mozambique Channel). *Org. Geochem.* **78**, 62–68 (2015).
29. K. Tanaka *et al.*, Quantification of NAD(P)H in cyanobacterial cells by a phenol extraction method. *Photosynth. Res.* **148**, 57–66 (2021).
30. G. M. Weiss, E. Y. Pfannerstill, S. Schouten, J. S. Sinninghe Damsté, M. T. J. van der Meer, Effects of alkalinity and salinity at low and high light intensity on hydrogen isotope fractionation of long-chain alkenones produced by *Emiliania huxleyi*. *Biogeosciences* **14**, 5693–5704 (2017).
31. E. F. Pai, P. A. Karplus, G. E. Schulz, Crystallographic analysis of the binding of NADPH, NADPH fragments, and NADPH analogues to glutathione reductase. *Biochemistry* **27**, 4465–4474 (1988).
32. H. W. Kreuzer-Martin, M. J. Lott, J. R. Ehleringer, E. L. Hegg, Metabolic processes account for the majority of the intracellular water in log-phase Escherichia coli cells as revealed by hydrogen isotopes. *Biochemistry* **45**, 13622–13630 (2006).
33. D. Sachse, J. P. Sachs, Inverse relationship between D/H fractionation in cyanobacterial lipids and salinity in Christmas Island saline ponds. *Geochim. Cosmochim. Acta* **72**, 793–806 (2008).
34. O. Dao, F. Kuhnert, A. P. M. Weber, G. Peltier, Y. Li-Beisson, Physiological functions of malate shuttles in plants and algae. *Trends Plant Sci.* **27**, 488–501 (2022).
35. T. D. Sharkey, Pentose phosphate pathway reactions in photosynthesizing cells. *Cells* **10**, 1547 (2021).
36. M. Giordano, J. Beardall, J. A. Raven, CO2 concentrating mechanisms in algae: Mechanisms, environmental modulation, and evolution. *Annu. Rev. Plant Biol.* **56**, 99–131 (2005).
37. J. R. Reinfelder, Carbon concentrating mechanisms in eukaryotic marine phytoplankton. *Ann. Rev. Mar. Sci.* **3**, 291–315 (2011).
38. A. R. Taylor, C. Brownlee, G. Wheeler, Coccolithophore cell biology: Chalking up progress. *Annu. Rev. Mar. Sci.* **9**, 283–310 (2017).
39. B. M. Hopkinson, A chloroplast pump model for the CO2 concentrating mechanism in the diatom Phaeodactylum tricornutum. *Photosynth. Res.* **121**, 223–233 (2014).
40. S. A. Kranz *et al.*, Low temperature reduces the energetic requirement for the CO2 concentrating mechanism in diatoms. *New Phytol.* **205**, 192–201 (2015).
41. J. N. Young, S. A. Kranz, J. A. L. Goldman, P. D. Tortell, F. M. M. Morel, Antarctic phytoplankton down-regulate their carbon-concentrating mechanisms under high CO2 with no change in growth rates. *Mar. Ecol. Prog. Ser.* **532**, 13–28 (2015).
42. N. Cassar, E. A. Laws, B. N. Popp, Carbon isotopic fractionation by the marine diatom Phaeodactylum tricornutum under nutrient- and light-limited growth conditions. *Geochim. Cosmochim. Acta* **70**, 5323–5335 (2006).
43. E. B. Wilkes, A. Pearson, A general model for carbon isotopes in red-lineage phytoplankton: Interplay between unidirectional processes and fractionation by RubisCO. *Geochim. Cosmochim. Acta* **265**, 163–181 (2019).
44. D. Pierrot, E. Lewis, D. W. R. Wallace, MS Excel program developed for CO_2 system calculations (CO2sys_v2.3xls) (Carbon Dioxide Information Analysis Center (CDIAC), Oak Ridge National Laboratory, U.S. Department of Energy, Oak Ridge, TN, 2006). 10.3334/CDIAC/otg.CO2SYS_XLS_CDIAC105a. Deposited 2006.
45. A. P. Cavanagh, R. Slattery, D. S. Kubien, Temperature-induced changes in Arabidopsis Rubisco activity and isoform expression. *J. Exp. Botany* **74**, 651–663 (2023).
46. S. Rabinowitch, N. B. Grover, B. Z. Ginzburg, Cation effects on volume and water permeability in the halophilic algae Dunaliella parva. *J. Membr. Biol.* **22**, 211–230 (1975).